JOURNAL OF PROPULSION AND POWER
Vol. 12, No. 5, September–October 1996

SP-100 Thermoelectric Cell Testing

Richard Ewell* and Andrew Zoltan†
Jet Propulsion Laboratory, California Institute of Technology, Pasadena, California 91109

Five prototypic SP-100 thermoelectric cells were put on test in vacuum at prototypic temperatures. Their thermal and electrical performances were characterized with 200, 300, 400, and 500°C temperature gradients across the cell. The latter was representative of prototypic operating conditions with a 1050°C hot-side temperature and a 550°C cold-side temperature. The initial thermal and electrical performance of all five cells closely matched predictions. Following the characterization testing the cells were put on an extended life test at the prototypic temperatures to determine any significant degradation modes of the cell. Throughout this test, the thermal performance of the cells was nearly identical to predictions. The tests with the initial three cells also confirmed earlier suspicions that the hot-side silicon–germanium-to-electrode interface would degrade without some significant protective coating at the bond line. Because of resource limitations and early development problems with this coating, the necessary protective layers had not yet been fully developed at the time the first three cells were manufactured. Subsequent to these tests, new cells were fabricated with this technology, two of which are currently on test. These two cells have not shown any significant degradation in performance beyond predictions. These tests along with accelerated experiments with coupons, have now validated the type-approval cell technology.

Introduction

IN March of 1983 the U.S. initiated the SP-100 Program to develop a space reactor power system capable of providing 10s to 100s of kilowatts of electrical power.[1] During the first three years of the program, system studies and critical feasibility issues were addressed to determine the lowest mass, 10-year life, and lowest cost space reactor power system to accomplish military and civilian missions. The result was the selection of a fast spectrum uranium nitride, lithium-cooled reactor coupled to thermoelectric energy conversion cells and heat pipe radiator panels to reject the waste heat to space. Since that time, considerable progress has been made in developing this space reactor power system.[2–5]

The SP-100 power conversion subsystem accepts heat from flowing lithium in the primary heat transport system, passes the heat through thermoelectric devices to produce power, and rejects the degraded heat through a lithium-cooled secondary heat transport system that is part of the heat rejection subsystem. The primary heat transport system, after 10 years of operation, would supply heat at temperatures up to 1375 K with a temperature drop through the hot-side heat exchanger of about 80 K. The secondary heat transport system accepts heat at about 850 K and returns the coolant at about 765 K.[6] Allowing for temperature drops within the heat exchangers, this results in a maximum temperature differential across the thermoelectric cells of 500 K.

The power converter subsystem consists of a number of power conversion assemblies, themselves consisting of several thermoelectric conversion assemblies. A power conversion assembly is a plate-and-frame device where the plates consist of arrays of thermoelectric cells (the thermoelectric conversion assemblies), and the frame consists of lithium-containing manifolds. The thermoelectric conversion assemblies produce the electricity for the SP-100. It is made up of conductively coupled multicouple thermoelectric cells that have a very high-power density compared with previous high-temperature thermoelectric technologies. The multicouple cells are metallurgically bonded to heat exchangers to achieve the high-power densities. This bonding introduces substantial mechanical stresses in the cells.

Test Objective and Purpose

The test program subjected prototypic SP-100 thermoelectric cells to a 500°C temperature gradient in a thermal vacuum environment. The test objectives were as follows:

1) Verify that the initial electrical and thermal performances of the cells were as predicted and understand any differences between the test data and predicted performance.

2) Validate that the cell degraded with time as predicted, and if there were any differences, determine the probable cause and decide what additional technology developments should be pursued.

Description of Test Articles

The thermoelectric cells that were tested are type-approval (TA) cells, and represent prototypic cells. The TA cells were fabricated and brazed onto hot and cold heat collectors and delivered to the Jet Propulsion Laboratory (JPL) for testing. The TA cell configuration is shown schematically in Fig. 1.[7] The cell was brazed to a niobium heat collector, on both the hot and cold side, to form the interface with the JPL test fixture. Cell 9 was the first cell fabricated with a porous niobium cold-side electrode and interconnect; previous cells had used porous tungsten.[8] Cells 30 and 31 were nearly identical to cell 9.[9] Cells 139 and 148 were fabricated subsequent to the completion of testing of the first generation of TA cells and included a thin coating of the low-voltage insulator material around the module perimeter and in the grooves of the module to prevent the loss of material from the hot-side silicon–germanium-to-electrode interface.

The TA cells consist of the following six components: 1) high-voltage insulator, 2) compliant pad, 3) low-voltage insulator, 4) electrode, 5) silicon–germanium (SiGe) multicouple stack, and 6) heat collectors. The high-voltage insulator is required to isolate the series connected cells from ground when they are put into the SP-100 system. Mechanical stresses in the thermoelectric cells were produced by manufacturing, from mismatches in the coefficients of thermal expansion of materials within the cell; thermal-gradient operation, from the

Received Nov. 22, 1995; revision received Feb. 5, 1996; accepted for publication March 6, 1996.

*Member of the Technical Staff, M/S 303-308, 4800 Oak Grove Drive. Member AIAA.

†Member of the Technical Staff, M/S 303-308, 4800 Oak Grove Drive.

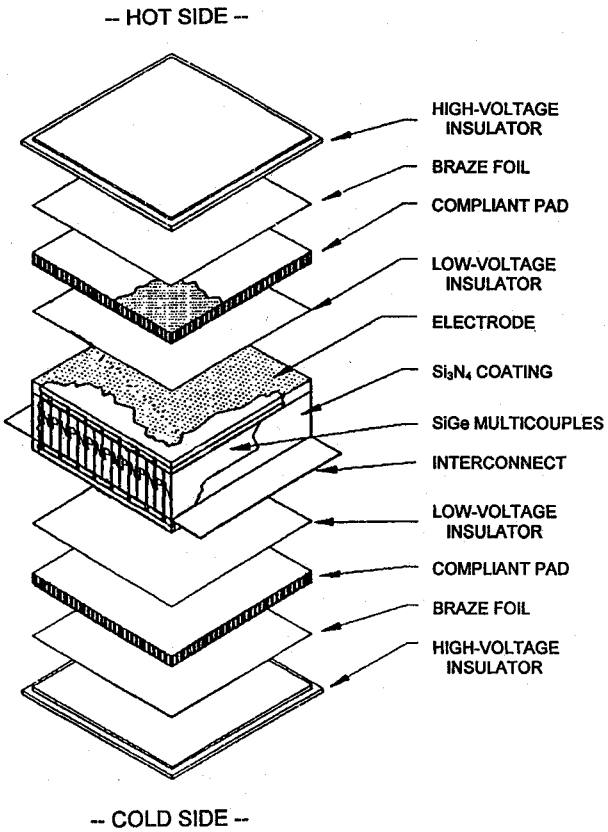

Fig. 1 TA cell configuration.

nonzero coefficient of expansion of the SiGe alloy; and thermal-gradient operation, from deflections between the hot and cold heat exchangers. Compliant pads isolated much of the stress from these sources while providing good heat transfer.

The low-voltage insulator is needed to electrically isolate the electrodes from shorting to the compliant pad. The electrode makes the series connection among the SiGe legs within the cell, and provided a means to electrically interconnect the cells on the cold side. The multicouple stack consists of alternating legs of *n*-type and *p*-type SiGe alloy that were bonded together by an insulating glass. There are eight *n*-type legs and eight *p*-type legs.

The hot-side heat collector was made of niobium to ensure that no material contamination of the cell could occur and to minimize the mechanical stress put into the cell from thermal expansion mismatches. The heat collector was a simple square plate attached to the hot end of the TA cell with the same braze used in the TA cell fabrication. The other side of the heat collector simply made a metal-to-metal low-pressure contact with the niobium base of the hot-side heater. The purpose of the heat collector was to minimize the temperature differential between the TA cell and the heater block. A large area ensured that even if the heat transfer was only accomplished by radiation, the temperature drop would still be less than 150°C. The actual measured temperature differential was about half this, indicating significant conductive heat transfer took place. This low-temperature differential was needed to minimize the heater temperature to ensure a long operating lifetime for the heaters. The heat collector was thick enough to be well instrumented with thermocouples, to facilitate the evaluation of the cell thermal performance.

The cold-side heat collector was also made of niobium to minimize cell stresses and ensure chemical compatibility. The TA cell was brazed to the cold-side heat collector similarly to the hot side. The cold-side heat collector also supported the power leads on either side of the cell. The porous niobium interconnects were bolted to solid niobium bars that were supported on boron nitride blocks that were bolted to the niobium heat collector. The side of the cold heat collector, opposite the cell, mated to the cold-side heater.

Description of Test Equipment

The test fixture, including the TA cell, was installed above a water-cooled copper base plate in a thermal vacuum chamber. The test fixture consisted of a hot-side heater, cold-side heater, fixture supports, and thermal insulation.

The hot-side heater block was fabricated from a niobium bar. The heater block contained four 150-W heaters. Each heater consisted of a molybdenum canister with a molybdenum heating element submerged into the canister. The heating element was insulated from the canister body with high purity alumina powder. The sides of the heater block were wrapped with 16 layers of dimpled molybdenum foil thermal insulation. A zirconia block was used to insulate the top side of the heater block. Fiberfrax, fibrous insulation, was placed above the heater to fill the void between the heaters and the zirconia insulator.

The cold-side heater was fabricated out of a niobium rod. The final shape of the cold-side heater resembled a spool. Tantalum wire was coiled around the inner part of the heater block to form the heater element. Alumina beads that were sectioned off from high-purity alumina tubes electrically insulated the heater wire.

The upper side of the cold-side heater interfaced with the niobium cold-side heat collector. There was a single layer of gold foil placed between the heater block and the cold-side heat collector to enhance the heat transfer between the two bodies. The lower side of the heater was resting on a water-cooled copper base plate. Sixteen type C thermocouples were used on the hot side, from the hot heater to and including the hot junction. Sixteen type E (chromel–constantan) thermocouples were used on the cold side. These were used from the cold junction down to the cold-side heater. During the testing of the final two cells, no thermocouples were used near the hot and cold junction to ensure the integrity of the protective coating around the module. Finally, for all of the cells, six voltage taps were attached.

The test and control rack consisted of the following components: alarm panel, DVM function panel, temperature function panel, load and load control panel, and the hot- and cold-side heater panels. The alarm panel was used to monitor and control system failure modes. Upon the detection of a loss of water coolant, loss of vacuum (pressure in excess of 8×10^{-4} torr), or major power interruption the system would interrupt the cell operation and shut down both the hot- and cold-side heaters to protect the thermoelectric cell from being damaged. In addition, both the hot- and cold-side heat-collector temperatures were monitored, and if either exceeded a set limit (1300°C at the hot side or 800°C at the cold side), the cell operation would be interrupted by shutting down the hot- and cold-side heaters.

The load and load control panel enabled the adjustment of the cell output power from short-circuit mode (I_{sc}) to open-circuit mode (E_{oc}). An open-circuit trigger circuit was installed to temporarily break the circuit to allow for measurement of the open-circuit voltage. The load controller allowed for the performance of parametric tests and the determination of the cell maximum power output. The load was controlled by a power supply in series with the cell and a shunt resistor. The shunt resistor was used to monitor the cell current.

The vacuum chamber was composed of a water-cooled stainless-steel bell jar, a cryogenic high-vacuum pump, and controller. The controller was connected to the alarm panel to provide for the safe operation of the cell. A vacuum of better than 5×10^{-6} torr was maintained throughout the test.

Test Procedure

Upon receipt of the TA cells a visual inspection was performed and the location of any visible cracks on the exterior

of the cell were noted. Color photographs were taken of each cell to document its status. The room temperature cell resistance was measured and a voltage map was made of the cell. All of the requisite thermocouples and voltage taps were attached to the cell, the cell was put into the test fixture, and the test fixture was put into the vacuum chamber.

The vacuum chamber was sealed and pumped down until a vacuum of less than 5×10^{-5} torr was obtained. Power was applied to both the hot- and cold-side heaters to heat the cell isothermally up to a uniform temperature of 550°C. At this point the cell resistance was measured. Then the power to the hot-side heater was increased and the power to the cold-side heater was reduced until a stable operating condition with a 200°C temperature differential across the cell was obtained. The cold-side cell temperature was 550°C and the hot-side cell temperature was 750°C. Once the cell was stabilized at this operating condition, steady-state data were taken for a minimum of five different load resistances. This was repeated with a 300, 400, and 500°C cell temperature differential. The temperature differential was increased by increasing the power to the hot-side heater and decreasing the power to the cold-side heater to maintain a cold-side cell temperature of 550°C. Following cell characterization the cell was put on extended test with a prototypic 500°C cell temperature differential.

Cell Performance Characterization Test Data

Although five cells were tested at JPL, cell performance characterization test data and analysis will only be presented for the first cell tested, TA cell 9. These test data are representative of the other four cells.

The first test done on the cell, following the initial verification of the test facility, was a parametric study of the electrical and thermal characteristics of the cell. The cell was tested at a minimum of five different load points with four different nominal temperature differentials across it. This first set of tests was done to determine the cell initial performance and find out how the cell performance compared to predictions.

During the initial characterization of the cell, comparisons were made between the predicted temperature profile and the actual thermocouple measurements. Figure 2 shows a comparison made at one of the 500°C data points for TA cell 9. The figure shows that there is an excellent match (within 4%) between the thermocouple measurements and the predicted temperature profile. The predicted profile was based on the input of a load resistance that gave a perfect match to the measured current. Hot- and cold-side fixture temperatures that closely matched those measured for the cell and give an exact match between the predicted open-circuit voltage and the measured open-circuit voltage were chosen. The predicted temperature profile matches the thermocouple measurements within the accuracy capability of the thermocouples. The only exception to this is within the SiGe legs themselves, and this is because the figure indicates a linear temperature gradient between the hot- and cold-junction temperatures, and this is not realistic. As a result of Peltier cooling at the hot junction and Peltier heating at the cold junction the actual profile will be nonlinear. The actual temperature near the hot-side thermocouple location should be below the prediction line and those near the cold junction should be above the prediction line. In both cases the thermocouple readings follow this trend.

During the initial characterization of the cell, comparisons were made between the predicted electrical performance of the cell and the actual measured current and voltage output of the cell. Figure 3 shows a comparison of the 500°C data points and the predicted current–voltage (I–V) cell characteristics. There is a reasonable match, however, as indicated by the slope of the I–V curve, the actual cell has a slightly higher internal resistance than was predicted. This is apparently the result of higher than predicted electrical contact resistances between the SiGe and the graphite of the electrode. Figure 4 shows a comparison of the 500°C data points and the predicted cell power output as a function of current. There is again a reasonable match, however, the measured peak power is slightly less (2.4%) than predicted and the power at high currents is lower than predicted. Similarly, this is the result of the higher-than-predicted cell internal resistance.

Extended Life Test

Following the completion of cell performance characterization under prototypic conditions, each cell was put on an extended life test with a fixed load at these same prototypic conditions. The extended life test was done to learn how the cell degrades with time, and to compare this degradation to predictions.

Cell 9 accumulated a total of 488 h of time on test with the hot-side temperature above 700°C because of the cell characterization tests, before it was put on extended life test. It remained on test for an additional 1800 hours, at which time the cell was taken off test and a destructive examination done.

The main deviation between the predicted cell performance and the actual cell performance over time was a result of a rapid increase in cell internal resistance. This is shown in Fig.

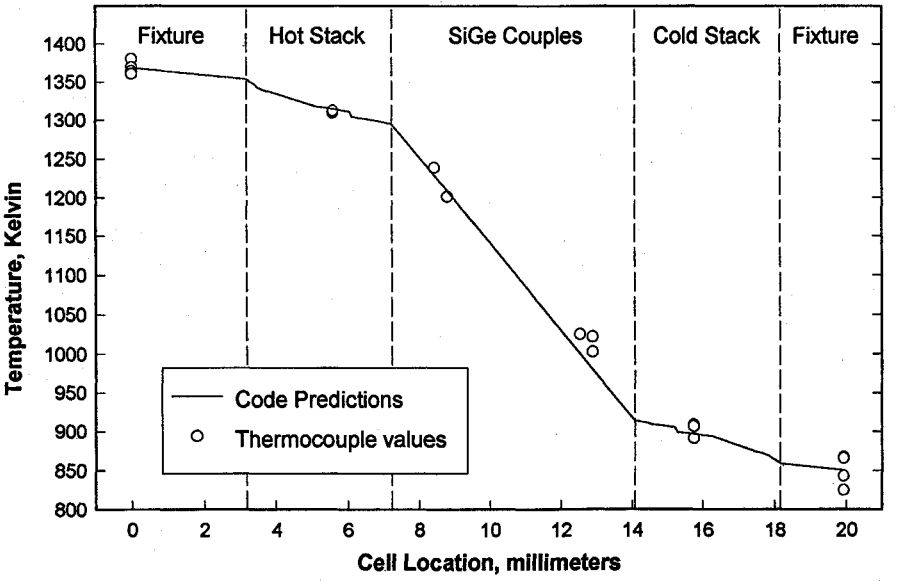

Fig. 2 Initial temperature profile comparison.

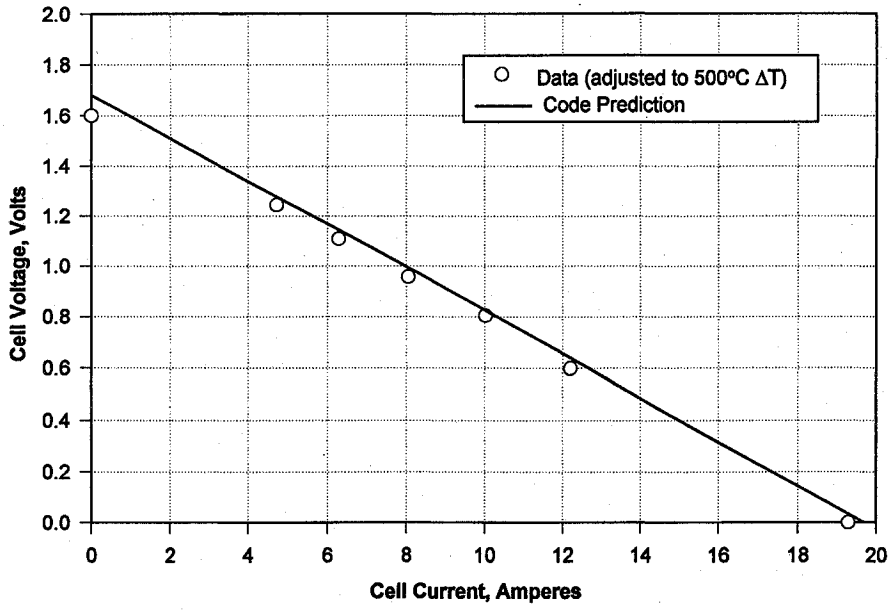

Fig. 3 Initial TA cell 9 I–V curve comparison at 500°C.

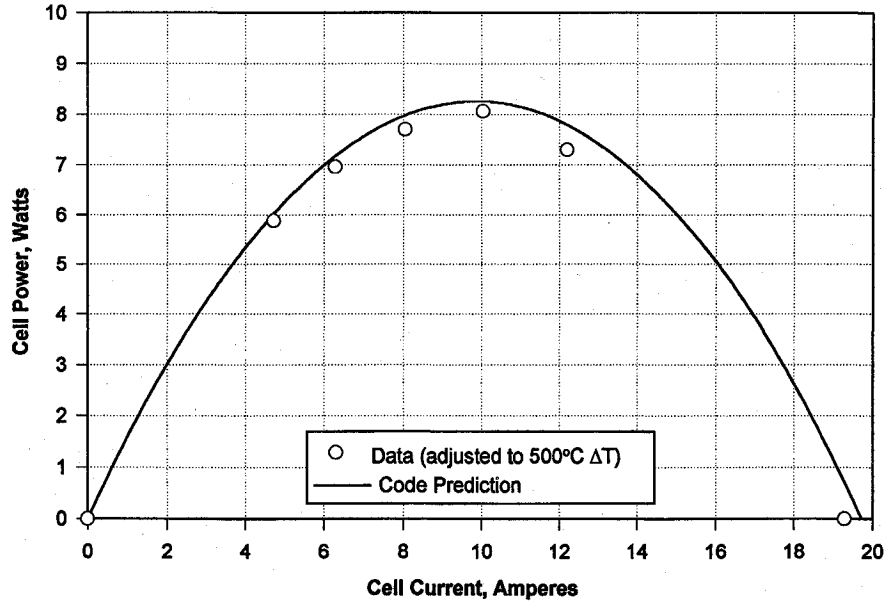

Fig. 4 Initial TA cell 9 I–P curve comparison at 500°C.

5, which shows the measured cell internal resistance as a function of time at temperature against the predicted increase that would result from dopant precipitation. The curve shows that the internal resistance increased by nearly a factor of 3 over the 2800 h of time on test. This compares to an expected increase of only 20% over this time period. This increase in cell internal resistance was the result of deterioration of the hot-side SiGe-to-graphite interface. This interface deteriorated so significantly that there was an actual separation between the outermost *n*-leg and the graphite on the hot side, as noted during the posttest examination.

Figure 6 shows the temperature corrected cell peak power output as a function of time. Two corrections were made: one to adjust the cell power to represent the power at the peak power voltage, and second to correct the power for temperature deviations away from the nominal 500°C operating point. The adjustment for the peak power is made by taking peak power to be as follows: power = $E_{oc}^2/(4*R_{int})$. This adjustment is reasonable if the cell is operating near the peak power current, so that the temperature would not change much in going to the peak power point. The temperature correction is P_{500} = (500/cell ΔT)^2*power. The plot shows that the cell power decreases considerably more than predicted. Again this is a result of the increased cell internal resistance.

Figure 7 shows how the cell thermal performance varies with time. It shows the deviation between the measured open-circuit voltage against the predicted open-circuit voltage. The prediction is based on using the measured fixture temperature and measured current as inputs to the code and using the assumed time dependence of the SiGe Seebeck coefficient. The figure indicates that there is excellent agreement between the two (within 5%). This shows that the thermal performance remained good throughout the duration of the test.

The other two cells of the initial group of three had similar degradation as cell 9. However, the two cells that were fabricated with the protective coating around the module, cells 139 and 148, did not have any degradation beyond that caused by normal SiGe dopant precipitation. The degradation in cell internal resistance as a function of operating time at temperature for these two cells is shown in Fig. 8. This figure shows that

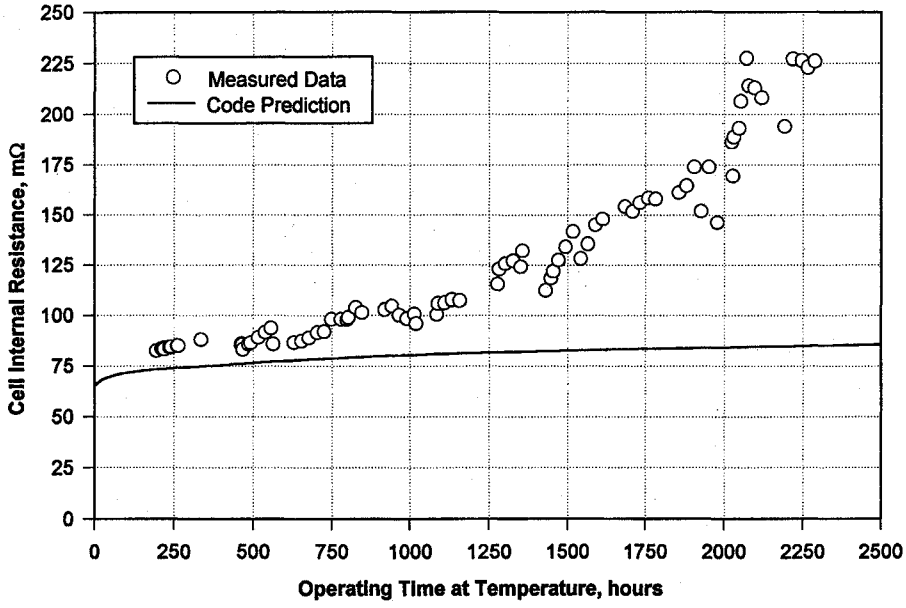

Fig. 5 TA cell 9 resistance degradation comparison.

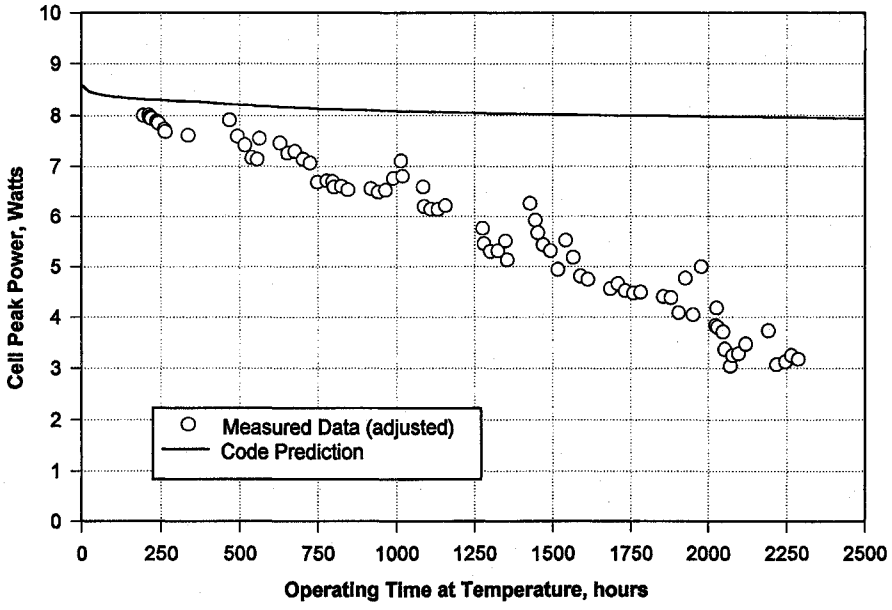

Fig. 6 TA cell 9 power degradation comparison.

after just over a year of time at temperature the degradation in internal resistance of both TA cells 139 and 148 closely follows a predicted curve based on dopant precipitation. All of the internal resistance data of cell 139 was within 3% of the predicted curve with a 17-mΩ resistance offset. In addition, coupon tests run at accelerated temperatures have demonstrated the equivalent of 11–13 years of operation without any apparent degradation. The other item to note from the figure is that the initial cell internal resistance is 17–21 mΩ greater than the code prediction. This was also found with many of the cells fabricated without the protective coating and is probably the result of a higher than optimal electrical contact resistance between the SiGe and the electrodes.

Post-Test Evaluation

After the TA cell 9 was taken off test at JPL, the cell was examined under an optical microscope and the cell resistance was mapped. Under an optical microscope it was evident that there was nearly a complete debond at the outermost *n*-type SiGe to graphite interface at the hot end on one side of the cell. No significant crack was observed on the other side, and it was not possible to see along the end to determine the extent of the crack.

Further evidence for the deterioration of TA cell 9 comes from a comparison of the room temperature voltage maps taken at the beginning and end of testing. By examining the initial voltage map it is apparent that the contact resistance between the SiGe and the graphite electrodes is approximately the same throughout the cell. Whereas, by examining the voltage map at the end of testing, it is apparent that the hot-side bond resistances have changed significantly, but the cold-side bond resistances are very similar to the beginning of test values. The outermost hot-side *n*-type SiGe/graphite bond resistance had gone up about 240 times over its initial value. The adjacent *n*-type SiGe/graphite bond resistance had increased by about 15 times over its initial value. The four central *n*-type SiGe/graphite bonds had their resistance increased by about four to five times their initial value. The resistance of

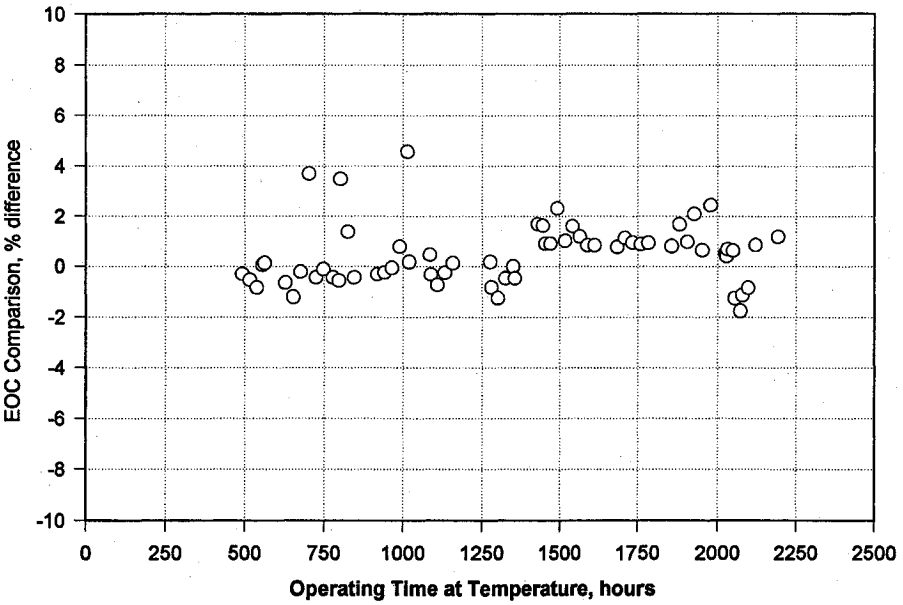

Fig. 7 TA cell 9 open-circuit voltage comparison.

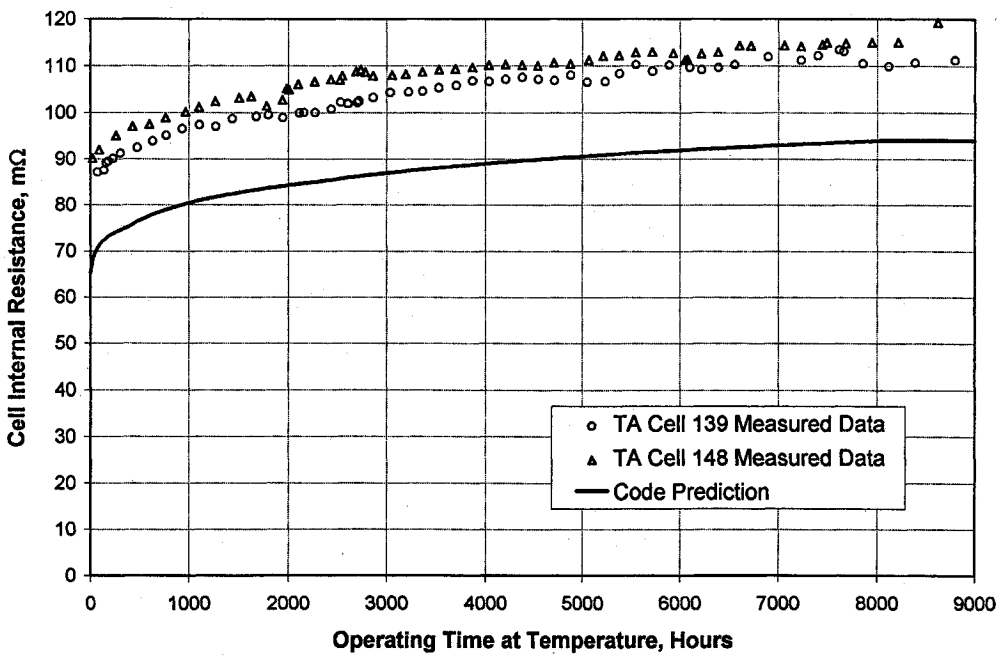

Fig. 8 TA cells 139 and 148 resistance degradation comparison.

the *n*-type SiGe/graphite bond for the couple with the outermost *p*-leg had a resistance increase of about 35 times. The resistance of the adjacent *n*-type SiGe/graphite bond had increased by about 13 times. This shows that the *n*-type SiGe/graphite bond deteriorates with time at temperature and that the outermost bonds are most affected. A similar deterioration occurred with the *p*-type SiGe/graphite bond, but to a much lesser extent. The bond where the *p*-leg was outermost had about a 20-fold increase in contact resistance as a result of time at temperature. The *p*-type SiGe/graphite bond, of the couple where the *n*-leg was outermost, had about a two times increase in electrical contact resistance. The six innermost *p*-type SiGe/graphite bond resistances were not significantly affected.

TA cells 139 and 148 have not yet undergone destructive evaluation, because they are still on test. They have not shown any unexpected degradation in performance with time at temperature, and so the problem with the deterioration of the SiGe/graphite bond appears to have been corrected.

Conclusions

The initial thermal and electrical performance of all five prototypic SP-100 thermoelectric cells tested was excellent. Their thermal performance was nearly identical to predictions. This shows that even with the large number of different layers that make up the SP-100 thermoelectric cell, excellent thermal performance is possible. This excellent thermal performance was maintained throughout the entire test period. The initial cell electrical performance, also, closely matched predictions. All five cells produced nearly 8 W of electrical power under prototypic conditions.

Following characterization testing, the cells were put on an extended life test at prototypic temperatures, to determine any significant degradation modes of the cell. Throughout this test,

the thermal performance of the cells was nearly identical to predictions. The first three cells tested confirmed earlier suspicions that the hot-side SiGe-to-electrode interface would degrade without some significant protective coating at the bond line. Subsequent to these initial tests, new cells were fabricated with a protective coating around the module and put on test. The two cells currently on test at JPL with this protective coating have not shown any degradation in the hot-side SiGe-to-electrode interface and have behaved exactly as predicted. This test and accelerated experiments with coupons have now validated the TA cell technology.

Acknowledgments

The research described in this article was carried out by the Jet Propulsion Laboratory, California Institute of Technology, under contracts with NASA and the Department of Energy. The five prototypic SP-100 thermoelectric cells were fabricated by Lockheed Martin Astro Space in Valley Forge, Pennsylvania.

References

[1]Mondt, J. F., Truscello, V. C., and Marriott, A. T., "SP-100 Power Program," *Proceedings of the 11th Symposium on Space Nuclear Power and Propulsion*, American Inst. of Physics, Albuquerque, NM, Jan. 1994, pp. 143–155.

[2]Truscello, V. C., and Rutger, L. L., "The SP-100 Power System," *Proceedings of the 9th Symposium on Space Nuclear Power and Propulsion*, American Inst. of Physics, Albuquerque, NM, Jan. 1992, pp. 1–23.

[3]DeMuth, S. F., "SP-100 Reactor Subsystem Development," *Proceedings of the 11th Symposium on Space Nuclear Power and Propulsion*, American Inst. of Physics, Albuquerque, NM, Jan. 1994, pp. 171, 172.

[4]DeMuth, S. F., "SP-100 Control Drive Assembly Development Plan," *Proceedings of the 11th Symposium on Space Nuclear Power and Propulsion*, American Inst. of Physics, Albuquerque, NM, Jan. 1994, pp. 173, 174.

[5]Buksa, J. J., "SP-100 Heat Transport Technology Development," *Proceedings of the 11th Symposium on Space Nuclear Power and Propulsion*, American Inst. of Physics, Albuquerque, NM, Jan. 1994, pp. 175–181.

[6]England, C., and Ewell, R. C., "Progress on the SP-100 Power Conversion Subsystem," *Proceedings of the 11th Symposium on Space Nuclear Power and Propulsion*, American Inst. of Physics, Albuquerque, NM, Jan. 1994, pp. 183–193.

[7]Bond, J. A., Matteo, D. N., and Rosko, R. J., "Evolution of the SP-100 Conductively Coupled Thermoelectric Cell," *Proceedings of the 10th Symposium on Space Nuclear Power and Propulsion*, American Inst. of Physics, Albuquerque, NM, Jan. 1993, pp. 753–758.

[8]Ewell, R. C., and Zoltan, A., "Final Report for the Ingradient Test of SP-100 Type Approval Cell 9," Jet Propulsion Lab., D-11486, Pasadena, CA, April 1994.

[9]Ewell, R. C., and Zoltan, A., "Final Report for the Ingradient Tests of SP-100 TA Cells 30 and 31," Jet Propulsion Lab., D-11703, Pasadena, CA, Aug. 1994.